ACS APPLIED MATERIALS & INTERFACES

Research Article

www.acsami.org

Kinetically Controlled Growth of Fine Gold Nanofractals from Au(I) via Indirect Galvanic Replacement Reaction

Yao Zhou and Hua Chun Zeng*

NUS Graduate School for Integrative Sciences and Engineering and Department of Chemical and Biomolecular Engineering, Faculty of Engineering, National University of Singapore, 10 Kent Ridge Crescent, Singapore 119260

Supporting Information

ABSTRACT: Two of the most important features of Au nanostructures, size and shape, are significantly affected by the reduction kinetics of the relevant metal precursors. Because of the high standard oxidative potential of gold ionic species, $AuCl_4^-$ in particular, Au fractals formed via various chemical or electrochemical approaches often have very coarse branches with diameters varying from tens of nanometers to submicrometers, even though extensive chemicals and/or complicated processes have been deployed to control the reduction kinetics. Herein we report an indirect galvanic replacement (IGR) strategy where the electrons generated in a galvanic replacement reaction from anode oxidation are channeled out to a separate conducting film on which the cathodic metal can be deposited. Reduction of Au(I) ionic species with relatively low standard oxidative potential has been conducted with the IGR experimental setting. 2D finely hyperbranched Au fractals (4.0 nm in diameter and a few micrometers in length) with high structural integrity were produced. Controls over the deposition density, location, and microfeatures of Au nanofractals were demonstrated through a mechanistic study. In addition, the thus-prepared Au nanofractals were also thoroughly tested in electrochemical sensing of H_2O_2.

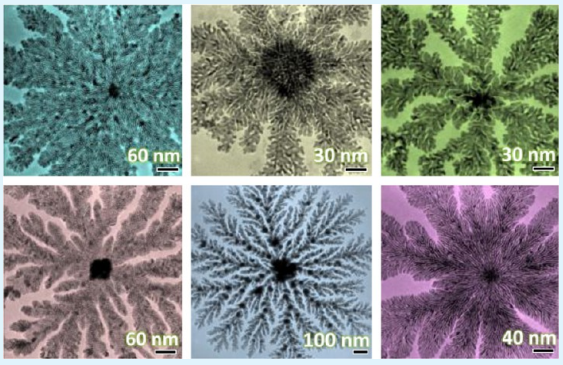

KEYWORDS: *gold nanofractals, interface reaction, reduction kinetic control, indirect galvanic replacement*

1. INTRODUCTION

Fractals or dendritic structures, whose growing patterns are self-similar in a statistical sense, have been frequently observed both in nature and in scientific research.[1−4] The formation process of dendritic structures is mainly dictated by three factors including ion transport, interface processes, and the crystalline anisotropy of a depositing matter. In recent years, in particular, dendritic nanostructures of Au with different levels of anisotropicity were formed through various methods.[5−8] As one of the most inert metals, properties of Au nanostructures largely depend on their sizes, which associate closely with the reduction kinetics.[9−11] In most wet chemical or electrochemical approaches, tetrachloroaurate ($AuCl_4^-$) was used as the precursor for growth of Au fractals. Nonetheless, because of its high standard oxidative potential, usage of $AuCl_4^-$ species is often associated with too fast reduction kinetics. Various strategies were employed to control the reduction kinetics for growth of Au fractals. For instance, supermolecular complexes of β-cyclodextrin and dodecyltrimethylammonium bromide,[12] organic electrolyte such as *N*,*N*-dimethylformamide/acetonitrile,[13] or agents such as ethylenediamine[14] were used in electrodeposition of Au fractals. Among various galvanic replacement reactions,[6,15,16] nonaqueous solvent such as highly viscous ionic liquid[6] was also employed. In addition, there is also a report on usage of thermally evaporated hexadecylaniline thin films as a substrate to control deposits of Au fractals.[16] In spite of the extensive chemicals and/or complicated processes employed, Au nanofractals produced through the above strategies nonetheless still have coarse branches with diameters from tens of nanometers to even submicrometers,[12,14,17] indicating limited control over the reduction kinetics of the metal precursor.

Meanwhile, galvanic replacement reactions represent one of the most important low-temperature methods for growth of various metal and even metal oxide micro-/nanostructures.[15,18−24] In most galvanic replacement reactions, the two half-reactions take place at the same location, or the dissolving anodic metal and the depositing cathodic metal are in direct contact. Such processes can be classified as direct galvanic replacement (DGR). The electrons generated from the anodic oxidation in a DGR process are consumed readily by the cathodic ions from the solution. Therefore, a DGR process is usually associated with relatively fast redox processes, which probably explains why Au nanofractals from such DGR process usually have coarse branches.[15,16] In addition, in a DGR process the anodic metal directly serves as a substrate for galvanic deposition of the cathodic metal, which therefore does not allow many choices of the surface properties of the substrate for the cathodic deposits.

Received: July 27, 2015
Accepted: September 11, 2015
Published: September 11, 2015

DOI: 10.1021/acsami.5b06818
ACS Appl. Mater. Interfaces 2015, 7, 21552−21561

Recently, we recognized that the galvanic replacement reactions occurring within a local electrochemical cell might offer advantage over the growth control of metal nanofractals when the anode and cathode are distanced in space by a conducting film. In this work, we used transmission electron microscopy (TEM) sample grids (e.g., Formvar/carbon-coated copper grid (FCCG)) to configure redox environments. On the conducting film (e.g., the Formvar layer and the carbonaceous layer in the case of a FCCG), with the precursor solution serving as the electrolyte, local galvanic cells would be established where the Cu grid is the dissolving anode and the anodic electrons flow to the conducting film that serves as a substrate for cathodic gold deposition. As such, this alternative process where the anode and the cathode are apart in space is termed as indirect galvanic replacement (IGR). Using this IGR strategy and Au(I) species prepared from redox reaction of $HAuCl_4$ and S^{2-}, facile and highly repeatable generation of fine Au nanofractals with diameters of 4.0 nm and length of micrometers has been realized. The formation mechanism was examined, and on the basis of this, controls over the growth density, formation location, and local features are also demonstrated. Performance of such fine Au nanofractals toward electrochemical sensing of H_2O_2 was also evaluated.

2. EXPERIMENTAL SECTION

2.1. Chemicals, Materials, and Apparatuses. The following chemicals were used as received without further purification: Na_2S (Alfar Aesar), $HAuCl_4{\cdot}3H_2O$ (>99.99%, Sigma-Aldrich), cetyltrimethylammonium bromide (CTAB, ≥ 99.6%, Fluka), $AgNO_3$ (>99.8%, Merck), ethanol (analytic-grade, Merck), methanol (analytic-grade, Merck), acetone (analytic-grade, Merck), H_2O_2 (30%, Merck), phosphate-buffered solution (PBS, pH 7.0, Merck), 5% w/w perfluorosulfonic acid−PTFE copolymer (nafion, Alfa Aesar), and ultrapure water (Merck Millipore); deionized water was collected through the Elga MicroMeg purified water system. Extra-thick FCCG (FCF-200-Cu, 200 mesh, Electron Microscopy Sciences), extra-thick Formvar/carbon-film-coated nickel grids (FCF-200-Ni, 200 mesh, Electron Microscopy Sciences), carbon-film-coated copper grids (CCG; CF-200-Cu, 200 mesh from Electron Microscopy Sciences), and extra thick Formvar/carbon-film-coated gold grids (FCF-200-Au, 200 mesh, Electron Microscopy Sciences). For the above three copper grids, the Formvar layer thickness is 25−50 nm, and the carbon layer thickness is 20−30 nm. UV−vis spectrometer (UV-2450, Shimadzu), transmission electron microscopy (TEM, JEM-2010, 200 kV), scanning electron microscopy (SEM, JSM-5600 LV), field-emission scanning electron microscopy (FESEM, JSM-6700F), field-emission transmission electron microscopy (FETEM, JEM-2100F, 200 kV), and X-ray photoelectron spectroscopy (XPS, AXIS-HSi, Kratos Analytical) were carried out as described below.

2.2. Preparation of Precursor Solution. Solution A is a mixture of 5.0 mL of deionized water, 1.0 mL of $HAuCl_4$ (0.01 M), and 1.0 mL of CTAB (0.1 M). Solution B, which is a colloidal Ag_2S solution, was prepared by mixing 0.1 mL of CTAB (0.1 M), 0.1 mL of Na_2S (0.1 M), and 0.2 mL of $AgNO_3$ (0.1 M) in 10.0 mL of deionized water. A portion of solution A is added into a portion of solution B to have the molar ratio of Ag_2S (or S^{2-}) to $HAuCl_4$ (R) varying from 0.2 to 4.0. The mixture was stirred at room temperature for at least 30 min. Afterward, the whole mixture was centrifuged at 6000 rpm for 25 min, and the transparent supernatant was obtained as the precursor solution for further use.

2.3. Galvanic Deposition of Gold. There were two general ways used in this work to conduct the galvanic deposition of Au. One way was accomplished by dropping some precursor solution on either side of the FCCG that was placed on a clean filter paper and dried naturally in open air. The side on which the solution was dropped showed little effect on the integrity of final gold fractal patterns because the dropped solution actually wetted both sides of the FCCG. The other way was to immerse the FCCG in a conical-bottomed centrifuge tube (maximum volume = 1.5 mL) filled with a proper amount of the precursor solution for a specific period of time, and then took it out. After washing with water and ethanol, the Au-deposited FCCG was dried naturally. Unless otherwise specified, the reaction temperature was room temperature at 23 °C. Such sample-loaded FCCGs were observed directly by TEM, SEM, and FETEM.

2.4. Sample Preparation for XPS Analysis. XPS analysis was conducted using a monochromatized Al Kα exciting radiation ($h\nu$ = 1286.71 eV) with a constant analyzer-pass-energy of 40.00 eV. All the binding energies (BEs) were referenced to the C 1s peak (BE = 284.5 eV) arising from C−C bonds. To analyze their chemical compositions, the precursor solutions with different R values were dropped respectively on a clean glass slide and dried at room temperature. This is because the glass is chemically inert and will not react with the precursor solution. To compare resultant chemical contents of the carbonaceous side and copper-grid side through XPS analysis, two pieces of pristine FCCG were immersed in the same precursor solution simultaneously and handled exactly in the same way in order to get identical reaction results. The resultant two FCCGs, one with its carbonaceous side facing-up and the other with its copper-grid side facing-up, were used for compositional comparison under the same XPS measurement conditions.

2.5. Sample Preparation for SEM/FESEM Analysis. To compare the products formed on the carbonaceous side and the copper-grid side, two pieces of identical product-loaded FCCG were prepared in the same way as described in the above XPS analysis. The carbonaceous side of one of the two FCCGs and the copper-grid side of the other were decorated with Pt coating and loaded for FESEM analysis under the same measurement conditions.

Apart from the above reactions and characterizations for FCCGs, when necessary carbon-film-coated copper grid, Formvar/carbon-film-coated nickel grid, and Formvar/carbon-film-coated gold grid were also used to replace FCCG under the reaction and analysis conditions.

2.6. Electrochemical Applications for H_2O_2 Sensor. A 1.0 mL aliquot of the precursor solution (R = 1.0) was transferred to a conical centrifuge tube with a volume of 1.5 mL into which a FCCG was added and allowed to sink to the bottom with the copper-grid side facing up. After storing the tube at 4 °C for 1.5 h, the precursor solution was removed, and the Au-nanofractal-loaded FCCG (Au-FCCG) was washed twice with water and ethanol. Before attaching the Au-FCCG onto the glass carbon electrode (GCE), the GCE was successively polished with 1, 0.3, and 0.05 μm alumina slurries on a polishing microcloth; the electrodes were sonicated in ultrapure water for 10 s between slurries. Afterward, the GCE was subjected to chemical polishing through anodization at +1.80 V (vs Ag/AgCl) in 0.1 M NaOH for 10 s and rinsed with ultrapure water.

To prepare the FCCG-GCE or Au-FCCG-GCE electrode, similarly a pristine FCCG or Au-FCCG was placed on a clean filter paper with the copper-grid side facing up; 2.0 μL of 0.5 wt % nafion aqueous solution was dropped on the above-polished GCE. The copper-grid side of FCCG or Au-FCCG was then adhered to the nafion-covered GCE. Subsequently, the excess nafion solution in the edge of FCCG or Au-FCCG was removed using a filter paper, followed by 4.0 μL of 0.5 wt % nafion aqueous solution being added on top of the electrode, which was then dried under ambient conditions.

Electrochemical measurements were conducted using a computer-controlled potentiostat (Autolab, PGSTAT 302N) with a standard three-electrode configuration. The counter and reference electrodes were Pt gauze and Ag/AgCl in saturated KCl, respectively. The above Au-FCCG-GCE or FCCG-GCE as the working electrode was first subjected to cyclic voltammetry scan within 0 to −0.4 V (vs Ag/AgCl) for 30 cycles with a scan rate of 50 mV/s in 10.0 mL of PBS (pH 7.0). Cyclic voltammograms without or with 2.45 mM H_2O_2 in PBS was obtained. The chronoamperometric response of the working electrode to different concentration of H_2O_2 was measured in 10.0 mL of PBS (pH 7.0) at constant potential of −0.2 V (vs Ag/AgCl). For the Au-FCCG-GCE, at every ca. 2 min, (at the early stage) 10 μL of 2.0 mM H_2O_2 or (at the later stage) 100 μL of 20.0 mM H_2O_2 aqueous solution was injected successively into the PBS. For the FCCG-GCE,

DOI: 10.1021/acsami.5b06818
ACS Appl. Mater. Interfaces 2015, 7, 21552−21561

at every ca. 2 min, 100 μL of 2.0 mM H_2O_2 was injected successively. Note that the H_2O_2 solutions were freshly prepared using deionized water purged with N_2 for 0.5 h. Baselines with steady-state signal were obtained prior to injection of H_2O_2, and the solution was mildly magnetically stirred.

3. RESULTS AND DISCUSSION

3.1. Formation of Au Nanofractals. Prior to galvanic deposition of Au nanofractals, preparation of the precursor solution is needed, which simply involves redox reaction of $HAuCl_4$ and S^{2-} at room temperature in the presence of CTAB.[25−27] The reaction mixture was centrifuged to get the clear supernatant. XPS (Figure S1), UV−vis (Figure S2), and TEM (Figure S3) investigation revealed that the chemical compositions of such supernatants vary depending on the initial reaction ratio of S^{2-} to $HAuCl_4$ (i.e., R). Supernatants prepared with R between 0.2 and 2.0 were used as precursor solutions for galvanic deposition of Au fractals, and their major active component is the complex between Au(I) and CTAX (X = Cl and Br, i.e., $CTA^+(AuX_2)^-$). (See Figures S1−S5 for detailed analysis on the composition of precursor solution.) Note that free S^{2-} ions are well-known to interact strongly with many heavy metals. Hence, to avoid interference from free S^{2-} ions in the following galvanic replacement reactions, solid Ag_2S rather than Na_2S was used as source of S^{2-} to partially reduce $HAuCl_4$ so that the resulting precursor solutions is almost free of S^{2-} ions (K_{sp} of Ag_2S is 1×10^{-51}). Besides Ag_2S, other oxidized sulfur species were also precipitated together with Ag^+ ions. Consistently, XPS analysis confirmed that silver and sulfur species are negligible in the precursor solutions with $R < 2.0$ (Figure S5).

Compared with many electrodeposition approaches that often involve tedious processing of electrode surface and optimization of the technical parameters, our approach is facile and highly repeatable. Simply by casting the above precursor solution on a FCCG, fractal patterns of gold were obtained after drying the sample grid naturally in open air. Specifically, fractals with high structural integrity were obtained from precursor solution with R values ranging from 0.6 to 2.0, and dilution of the precursor solutions with deionized water indicated no noticeable effect on the structural integrity of nanofractals. As shown in Figure 1a, most fractal patterns are rather symmetric, with their diameters varying from micrometer to submicrometer scale (Figure 1b,c). Each of these fractals consists of numerous wires with uniform diameters of around 4.0 nm and with lengths as large as micrometers extending from the center in a radiant manner (Figure 1d,e,f). As a typical feature of fractals, dendritic stems began emerging at different points and underwent repeated tip-splitting, forming a large number of Y junctions projecting outward (Figures 1c and S6). Centers in most of the fractals are much darker (in TEM images) than their outer regions. The fractals are polycrystalline in nature (HRTEM; Figures 1g and S6) and consist of randomly oriented domains a few nanometers in size. A number of lattice fringes (0.24, 0.20, and 0.14 nm) were observed that correspond to d_{111}, d_{200}, and d_{220} of Au. In particular, 0.24 nm was found to have the highest statistical significance. Elemental mapping (Figure 1h) and XPS analysis (presented in Figure 3a) revealed that the fractals are indeed metallic gold. Au fractal patterns with comparable integrity and anisotropy could also be obtained when immersing a FCCG into the precursor solution for some time and/or using a carbon-coated copper grid (CCG; Figure S7) in replacement of

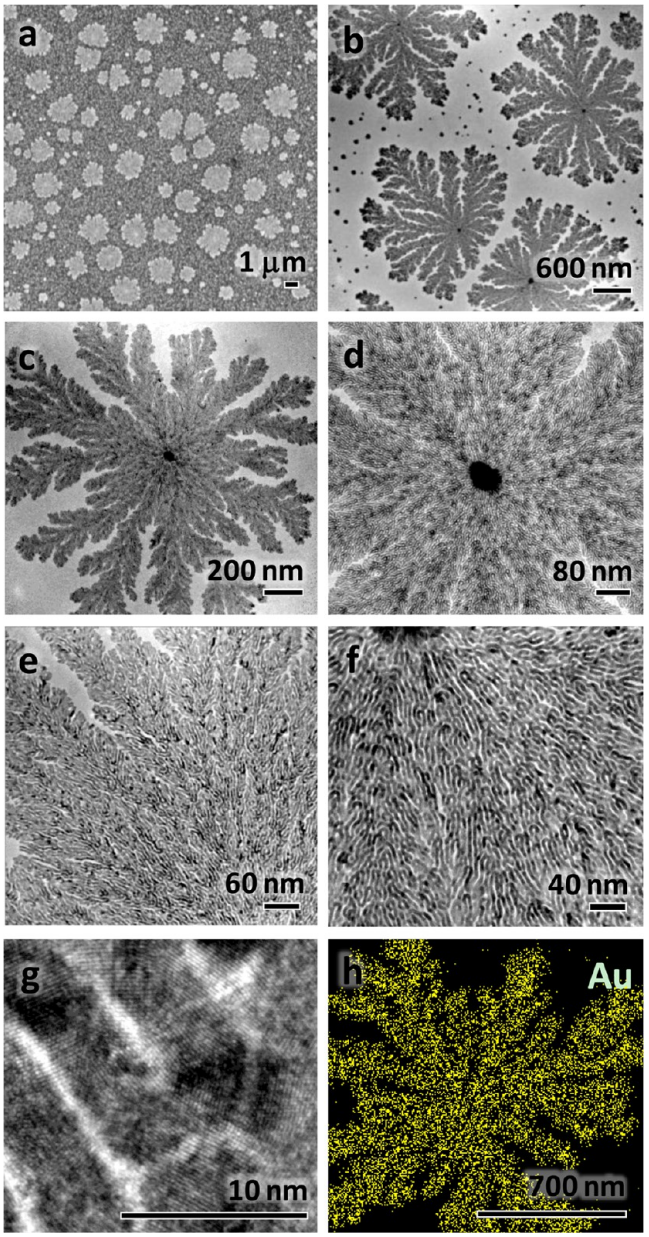

Figure 1. Typical Au nanofractals formed on the carbonaceous side of a FCCG through IGR processes: (a) FESEM image, (b−f) TEM images at different magnifications, (g) HRTEM image, and (h) elemental mapping of Au.

a FCCG. All of the fractals produced out of this IGR process are formed on the Formvar/carbon film, and the branches of the Au nanofractals exhibit a much higher level of anisotropicity than those prepared through aforementioned electrodeposition or DGR process whose branches usually range from a few hundreds of nanometers to even micrometers wide.[7,13,22−24] (Note that TEM cannot reveal sample objects residing on the copper grid.)

3.2. Mechanistic Study of Formation of Au Nanofractals. To understand the chemical interaction between the metal grid and Au(I) species in the precursor solution, in Figure 2, both sides of a precursor-solution-treated FCCG, namely, the carbonaceous side and the copper-grid side, were subjected to XPS analysis. Signals of Au were found on both sides of the FCCG, and they are largely present in the metallic

DOI: 10.1021/acsami.5b06818
ACS Appl. Mater. Interfaces 2015, 7, 21552−21561

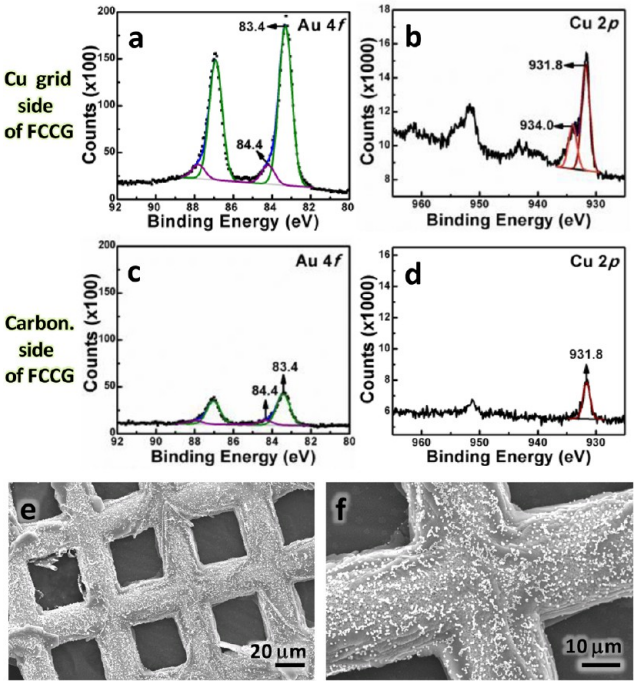

Figure 2. XPS spectra of (a and c) Au 4f and (b and d) Cu 2p measured on the copper-grid side (a and b) and on the carbonaceous side (c and d) of a FCCG treated with the precursor solution. The black dots/lines are the original experimental data, and the colored peaks are calculated data. BEs shown are only for Au $4f_{7/2}$ and Cu $2p_{3/2}$ branches. (e and f) Typical SEM images of deposits formed on copper grids of a CCG after reacting with the precursor solution.

state Au(0) as identified by a main peak at 83.4 eV (Figure 2a,c), together with that of CTAB (Figure S8). Note that typical BE peaks of the Au(I) species in the precursor solution is 84.5 eV (Figure S1a). Meanwhile, Cu(I) was also detected on both sides, with a Cu $2p_{3/2}$ peak at 931.8 eV (Figure 2b,d).[28] It should be mentioned that no signal of Cu species on the carbonaceous side could be detected when an as-received FCCG was referenced in the same XPS analysis. At the copper-grid side, in addition to Cu(I), one more Cu $2p_{3/2}$ peak at 934.0 eV and a satellite peak, which is a unique feature of Cu(II) species, are observed.[29] Depicted in Scheme 1, the conversion of Au(I) to Au(0) and the presence of both Cu(II) and Cu(I) species elucidated the occurrence of galvanic reactions between Au(I) species and the copper grid, in which copper serves as an anodic metal. Consistently, SEM observation of a FCCG or CCG treated with the Au(I) solution revealed dense granular particles adhered on the copper grid (Figure 2e,f), which verified the anodic reactivity of the copper to reduce the Au(I) species in this redox reaction. Evidently, as shown in Scheme 1, the dense aggregates residing on the copper grid (Figure 2e,f) were formed out of a DGR process where the Au(I) species were directly reduced and deposited on the surface of metallic copper grid.

Scheme 1. Illustration of Configuration (Side View) and the Two Processes of a Formvar/Carbon-Film-Coated Copper Grid (FCCG)[a]

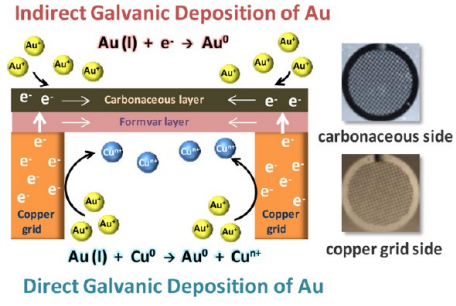

[a]White arrows indicate the flow direction of electrons; the blue and yellow spheres indicate copper and gold ions, respectively. The photographs on the right are the views from the top of the two sides of a commercial FCCG.

Formation of such fine Au nanofractals on the Formvar/carbon film (Figure 1) and the oxidation of copper grid (Figure 2) are direct proof for the occurrence of the IGR process illustrated in Scheme 1 where the two half-reactions of the overall redox reaction between Cu(0) and Au(I) were partitioned into two separate spaces. This is enabled by the electrically conductive Formvar/carbon film of a FCCG. (Point-contact measurement for this film is below 0.3 Ohm, as shown in Figure S9.) Therefore, a galvanic cell was formed where the solid Cu grid works as an anode, the Au nanoclusters nucleated at early stage on both sides of the conducting film as starting points for cathodic reduction, the precursor solution functions as the electrolyte, and the Formvar/carbon functions as a conducting medium to transport anodic electrons generated. Driven by the potential difference, a continuous flow of electrons from Cu(0) to the Au(I) through the Formvar/carbon layers leads to the depositing growth of Au(0) on the conducting film of the FCCG. In such an IGR process, the cathodic reduction of Au(I) is governed by the anodic electrons within the local electric cells, which means that the reduction kinetics is partly dictated by the instantaneous local reducing potential of the microcathodes. Consistent with the IGR protocol, the self-limited growth behaviors were widely observed among closely neighbored nanofractals (Figure 3a) or among any intrabranches within the same nanofractal (Figure 3b). All the nanofractals grew in a self-constrained manner (Figures 1a and 3a), and within the same nanofractal, no branches entangle with others from a different stem (Figure 3b). More interestingly, these growing fractals tended to occupy all possible spaces, resulting in less symmetric final structures. As exemplified in Figure 3a, the nanofractal that is surrounded by three nanofactals exhibits a triangle-like pattern. The hyperbranches of these Au nanofractals can be considered as numerous microcathodes that possess instantaneous negative electrical potential because of the continuous flow of electrons generated from the anode oxidation. As illustrated by the red arrows in Figure 3a,b, at the boundary area of two growing

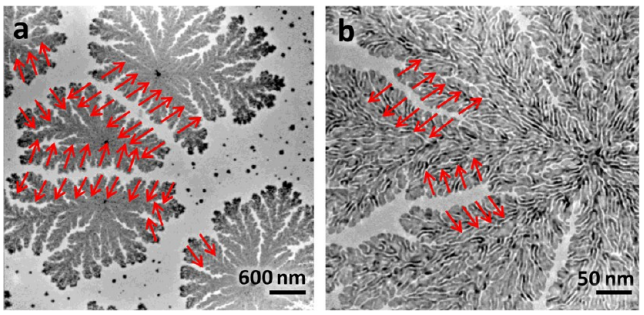

Figure 3. Typical self-limiting behaviors (a) among neighboring nanofractals or (b) among the branches within a nanofractal.

DOI: 10.1021/acsami.5b06818
ACS Appl. Mater. Interfaces 2015, 7, 21552−21561

nanofractals, one can expect (i) instantaneous electrostatic repulsive forces between the two neighbors and (ii) competition between the two neighbors toward Au(I) supply. Dominated by such Coulomb repulsion, similarly, it seemed to be prohibitive for the hyperbranches within the same fractal to join each other. Because of rapid consumption of the Au(I) species, in the vacant area between two close neighbors no new nanofractals or nanoparticles could be further deposited.

Interestingly, as depicted in Figure 4c, we found that under all our studied conditions no matter whether a FCCG or a

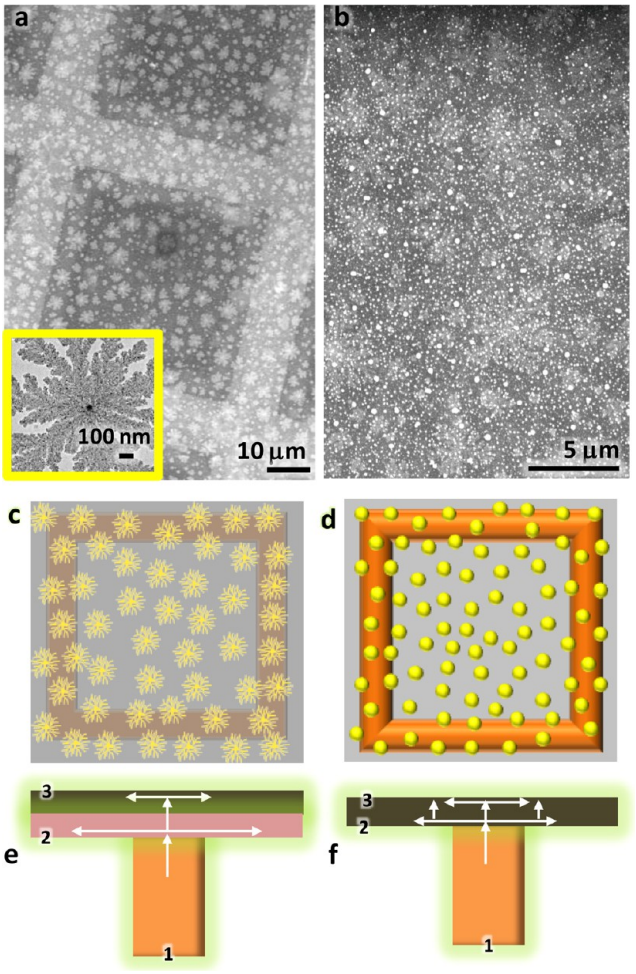

Figure 4. SEM images and schematic depictions of (a and c) Au nanofractals formed on the carbonaceous side and (b and d) granular aggregates formed on the copper-grid side when a CCG was used. Inset in a is the corresponding TEM image of the as-formed Au nanofractals. (e and f) Flow directions of anodic electrons within (e) a FCCG or (f) a CCG, where the numbers (1−3) denote the three interfaces involved and the white arrows indicate the flow of electrons.

CCG was used the Au nanofractals were exclusively formed on the carbonaceous side (Figure 1 for the FCCG case and Figure 4a for the CCG case; i.e., interface 3 depicted in Figure 4e,f). However, as shown in Figure 4d, on the copper-grid side (i.e., interface 1 or 2 in Figure 4e,f), only irregular or granular aggregates were formed. (See Figure 6e later for the FCCG case and Figure 2e,f and Figure 4b for CCG.) As illustrated in Figure 4e,f, because of the internal resistance of conducting film and actual configuration of FCCG or CCG, there will be an ohmic drop from interface 1 to interface 2 and then to interface 3, which will have decreasing instantaneous reducing potential during the reaction, even if the external chemical environments at the two sides of the FCCG or CCG are the same as those at the beginning of the reaction. Because higher reducing potential normally results in fast reduction of cathodic ions, we can deduce that the formation of Au nanofractals on interface 3 likely is favored by slow redox kinetics in the IGR process.

The preparation of Au(I) species with relatively low standard oxidative potentials also contributes to successful control over the reduction kinetics and thus the formation of such hyperbranched Au nanofractals. For a comparison, different gold ionic species were used as precursor solutions. In Figure 5a−c, products with evidently increasing levels of anisotropicity

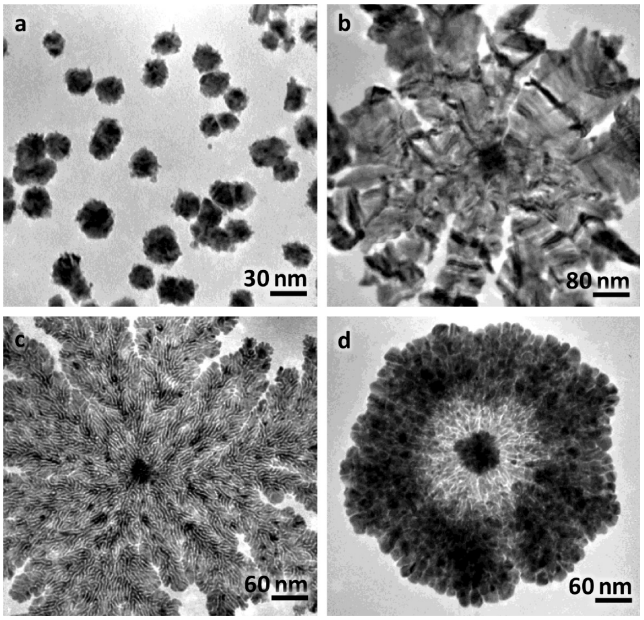

Figure 5. Cathodic deposits formed through IGR processes when a FCCG reacted with (a) 0.1 M $HAuCl_4$ aqueous solution, (b) mixture solution of $HAuCl_4$ and CTAB with a molar ratio of 1:2, and (c) the precursor solution containing Au (I) species. (d) Formvar/carbon-film-coated nickel grid reacted with the precursor solution containing Au(I) species.

were obtained: granular particles for the case of $HAuCl_4$ (Figure 5a), large flattened petals for the case of mixture of $HAuCl_4$ and CTAB (Figure 5b), and the hyperbranched nanofractals for the case of Au(I) (Figures 1 and 5c). Accordingly, the oxidation potentials of these precursor solutions can be ranked as follows: $HAuCl_4$ aqueous solution > mixture solution of $HAuCl_4$ and CTAB > Au(I). Moreover, the metal grids with different reducing potentials to react with the Au(I) species give a similar trend. When an extra-thick Formvar/carbon-coated nickel grid was used, circular fractal patterns with lower local anisotropy and structural integrity than those prepared by FCCG/CCG resulted (Figures 5d and S10). It is understandable that nickel has a much lower standard electrode potential ($E^\circ(Ni^{2+}/Ni^0)$ = −0.27 V) than that of copper ($E^\circ(Cu^{2+}/Cu^0)$ = 0.34 V and $E^\circ(Cu^{+}/Cu^0)$ = 0.52 V), and it can be oxidized more easily by Au(I) ($E^\circ(Au^{+}/Au^0)$ = 1.68 V). Note that no fractals can be formed when a Formvar/carbon-coated gold grid was used because thermodynamically the gold grid is too inert to be oxidized by the Au(I).

The formation of Au nanofractals with high local anisotropicity favored by slow reduction kinetics could be understood by the flow of the anodic electrons within the local

DOI: 10.1021/acsami.5b06818
ACS Appl. Mater. Interfaces 2015, 7, 21552−21561

cell. According to the "protruding effect", the electron density is higher (thus having a more negative potential) at the protruding part than in the rest parts of an anisotropic nanostructure[30,31] (e.g., at the tips of nanowire-shaped branches).[32,33] Hence, at a threshold point, the local field potential at the tips of nanobranches is more negative than other locations of the same branches. As such, reduction of Au(I) and deposition of Au(0) will preferentially occur at the tip regions, leading to the propagation of the nanobranches without much altering their diameters. Nonetheless, when the electron density is so high that the reducing potentials at both the tips and other parts of the branches are also more negative than the required reducing potential of Au(I) species, the reduction and deposition of Au(0) will occur in a less selective manner, resulting in structures with lower or no anisotropy.

In this sense, we attribute the formation of Au nanofratals with high local anisotropicity and structural integrity to "softer" and slower reduction of Au(I). The usage of the IGR experimental setting with inherent electrical resistance and Au(I) species with relatively low oxidative potential enabled the realization of slow reduction kinetics. This significantly differentiates our Au nanofractals with much finer branches from those produced through electrodeposition and/or DGR process.[22−24]

As depicted in Scheme 1, because of continuous dissolution of the Cu grid and limited mass transport at the copper-grid side, there might be a buildup of Cu^{2+}/Cu^{+} ions at the copper-grid side, resulting in a solid−liquid interface different from that at the carbonaceous side. For instance, accumulation of Cu^{2+}/Cu^{+} ions might inhibit the motion of Au(I) toward this interface, and the high ionic strength might even destabilize the Au deposits formed on site. As such, the deposition of the Au (I) at copper-grid side (i.e., interface 2) might be disturbed and the ultimate morphologies of the Au deposits are affected. In this sense, an IGR process can quarantine the cathodic deposition from the anodic oxidation via the conducting film, which avoids the disturbance of the dissolved anodic ions and provides a relatively clean surface for the cathodic deposition.

3.3. Controls over the Density, Formation Position, and Microfeatures of Au Nanofractals. Understanding the formation mechanism of Au nanofractals within an IGR setting enables control over the deposition density, the deposition location, and the local features of thus-formed Au nanofractals. First, the macroscopic chemical and physical environments at the two sides of an IGR system can be differentiated deliberately. As a simple demonstration, a FCCG is positioned at the bottom in a cone-shaped container filled with the precursor solution, with either the carbonaceous side facing up (Figure 6a) or the copper-grid side facing up (Figure 6b). Specifically, when a cone-shaped centrifuge tube with a volume of 1.5 mL was used, the FCCG (with a diameter of 3 mm) would sink to the deep bottom, dividing the precursor solution into a more or less isolated bottom portion with a volume of less than 10 μL and an upper portion with a large volume of around 1.49 mL (Figure S11). When the reaction proceeds, the Au(I) species in the bottom portion (<10 μL) will be consumed significantly. As a result, the side facing down will experience slower reduction kinetics. In comparison, the side facing up will always experience profuse amounts of Au(I) species because of the continuous transportation of the Au(I) species from the adequate bulk solution (1.49 mL) driven by the concentration difference. Therefore, most electrons will be directed to the side facing up where they are consumed readily

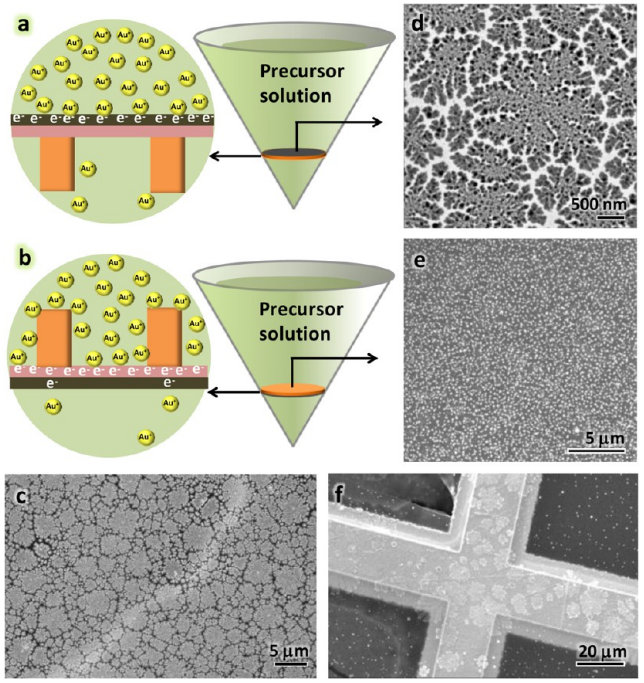

Figure 6. A FCCG is positioned in a cone-shaped container filled with the precursor solution: (a) copper-grid side of a FCCG faces down whereas the carbonaceous side faces up and (b) copper-grid side of a FCCG faces up whereas the carbonaceous side faces down. (c) SEM image and (d) TEM image of dense Au nanofractals formed on carbonaceous side in the case shown in a; (e) SEM image of dense granular particle aggregates formed on the copper-grid side and (f) sparse Au fractals formed on the carbonaceous side in the case shown in b.

by Au(I) species, whereas much fewer electrons are on the side facing down because of there being fewer electron acceptors (Au(I); Figure 6a,b). As such, the deposition of Au(0) on the side facing up would have faster reduction kinetics and thus more cathodic deposits. Hence, this enables a control over the growth density of Au nanofractals. The efficiency of such a strategy was well-confirmed by our experiments. When the carbonaceous side was facing up (Figure 6a), dense fractal patterns were formed over the entire carbonaceous side (Figure 6c,d). However, when the copper-grid side was placed upward (Figure 6b), only sparse fractal patterns were formed on the carbonaceous side (Figure 6f), whereas dense granular particle aggregates were formed on the copper-grid side (Figure 6e). Such comparative cathodic depositions under differentiated reaction environments were also confirmed using a CCG (Figure S12). Note that the deposition on either side of the film can be easily terminated by washing the FCCG (or CCG) with a mixture of deionized water and ethanol immediately after they were taken out of the precursor solution.

Furthermore, when a FCCG was treated according to the setting in Figure 6b, occasionally selected deposition of gold can be achieved, as observed in Figure 7a,b. As depicted in Figure 7c, region 2′ in the Formvar layer or region 2 in the carbonaceous layer is the area in contact with the copper grid underneath; they bridge the copper grid (region 1) with other parts of the conducting films (regions 3′ and 3). In the setting of Figure 7c, any generated electrons from region 1 would flow via region 2′ to region 2 in the carbonaceous layer. Electrons arriving at region 2 would either react with Au(I) species or flow to region 3. Therefore, with limited Au(I) species at the

DOI: 10.1021/acsami.5b06818
ACS Appl. Mater. Interfaces 2015, 7, 21552−21561

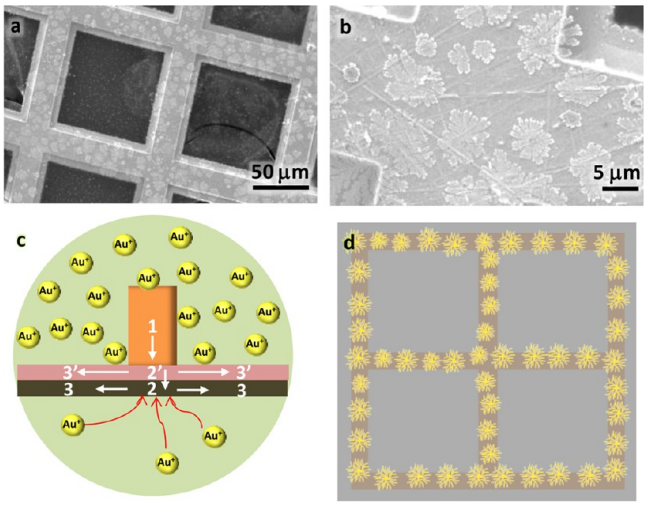

Figure 7. (a and b) SEM images (taken at different magnifications) of a pattern of Au nanofractals formed on the carbonaceous side of a FCCG treated according to Figure 6b, (c) schematic depiction of different regions (indicated by numbers) within a FCCG, and (d) schematic depiction of a pattern of Au nanofractals formed on the carbonaceous side.

carbonaceous side (Figure 6b), between the two locations (i.e., regions 2 and 3), Au(I) ions would preferably deposit at region 2, resulting in the pattern depicted in Figure 7d. The observation of such patterns is direct evidence reflecting the flows of anodic electrons within the IGR process.

The above-selected deposition of gold was only observed using a FCCG. When a CCG was positioned in the same manner as that depicted in Figure 6b, the Au nanofractals were formed nonselectively in both regions 2 and 3, as shown in Figure 4a. This is because the CCG, without a Formvar layer, has lower ohmic drop than the FCCG in all the directions. The anodic electrons can flow easily from region 3′ to 3. Therefore, in the CCG case, regions 2 and 3 would have comparable surface concentrations of electrons for Au(I) reduction. By changing the film composition (i.e., resistivity) or configuration, apparently one can further control the reduction kinetics.

Moreover, the local features of the Au nanofractal could be modulated by adjusting the recipe of the precursor solution. In our precursor solution, CTAX (X = Br or Cl) is essential to ensure fine fractal growth because it slows down the redox reaction between Au(I) and Cu(0) effectively by forming complexes with Au(I).[33] It may also serve as a transporting electrolyte to connect the cathode and the anode externally in bulk solution. Besides, it could contribute to the morphological control of nanowires in the fractal pattern by selectively adsorbing on specific facets of Au.[34] In fact, beltlike nanostructures rather than nanowires were formed when increasing amounts of additional CTAB were added to the original precursor solution (Figure 8a–c). In almost all of the fractal patterns we studied, the shapes of branches (Figure 1e), while extending from its center outward to their terminal points, changed from a wirelike (Figures 1f and 8a) to a beltlike crystal morphology (Figure 1e,g) that is similar to the branches prepared using high CTAB concentrations (Figure 8b,c). Such a phenomenon implies that the center (black spots in TEM images) of each individual fractal pattern is indeed a starting point and that their higher ordered branches are simply projected from this center in 360°. For example, when the

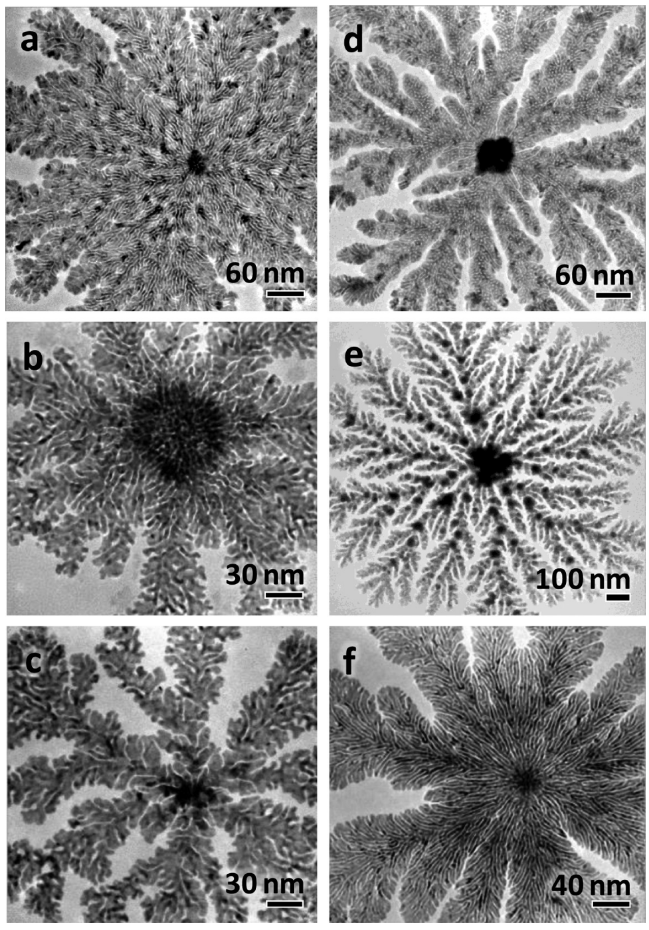

Figure 8. Different gold fractals formed from mixtures of 1.0 mL of the precursor solution with (a) 0 μL, (b) 50 μL, and (c) 100 μL of 0.1 M CTAB solution as well as with (d) 1.0 mL of methanol, (e) 1.0 mL of ethanol, and (f) 0.5 mL of acetone.

precursor solution was just dropped on a FCCG, the local concentration of CTAB was equal to that of the pristine precursor solution, and nanowires were formed through kinetically controlled reduction of Au(I) to Au(0). With the reaction proceeding on, however, both consumption of $(AuX_2)^-$ and evaporation of solvent would increase the concentration of CTAB. As a result, local concentration of CTAB would increase starting from the central point and reach a higher level at the terminating stage of fractal growth. This explains why the morphology of the branches at the peripheral areas resembles those produced with a high concentration of CTAB.

By modifying the solubility of CTAB in the solvent, the local features of fractal patterns could be tuned. When methanol was added into the precursor solution with a volume ratio of 1:1, the main structures of fractal pattern still existed. However, each main stem seems to become a porous network formed by numerous interconnected short-segmented wires (Figure 8d). By mixing 1.0 mL of ethanol with 1.0 mL of the precursor solution, snowflake patterns were produced, and their branches consist of many irregular crystal aggregates (Figures 8e and S13). When less ethanol was added (i.e., 0.5 mL) into 1.0 mL of the precursor solution, the patterns produced were similar to those produced using methanol. In contrast, when 0.5 mL of acetone was added into 1.0 mL of the precursor solution, ultrafine fractal patterns were observed (Figure 8f). Because

DOI: 10.1021/acsami.5b06818
ACS Appl. Mater. Interfaces 2015, 7, 21552−21561

solubility of CTAB in methanol or ethanol is much higher than that in water and acetone, the addition of methanol or ethanol increases the solubility of CTAB in the solvent, which can influence the fractal formation by the following two aspects. First, it leads to the dissociation and release of Au(I) from the complex of $CTA^+(AuX_2)^-$, speeding up the rate of galvanic reaction between the Au(I) and Cu(0). Second, the methanol or ethanol solvent weakens the capping effect of CTAB toward the gold nanofractals because more CTAB molecules were dissolved in the solvent. Hence, instead of long and branching nanowires, connected wires or larger crystal aggregates were formed, depending on the amount of methanol or ethanol added.

3.4. Electrochemical Applications for H_2O_2 Sensor. Because the hyperbranched Au nanofractals with these fine polycrystalline Au nanowires are formed in situ on the conducting film supported on a metal grid, the whole setting is highly conductive, which therefore provides a convenient platform for construction of electronic devices such as sensors. Herein, as a demonstration, a Au-FCCG-GCE was constructed with the copper-grid side in direct contact with the GCE and the carbonaceous side exposed to the solution, as shown in Figure 9b. Because the FCCG and GCE have the same diameter of 3 mm, they overlap perfectly with each other. CVs of the two electrodes in the absence and presence of H_2O_2 were obtained within 0.0 to −0.4 V (vs Ag/AgCl, similarly thereafter). For the FCCG-GCE, there is no anodic peak in the backward scans of the CV either in the absence or the presence of H_2O_2 (curves 1 and 2 and inset (expansion view of *I*), Figure 9c). This indicates no occurrence of electrooxidation of the copper because the anodic peak for electrooxidation of copper in PBS at pH 7.0 generally occurs at around 0.0 V.[35] This is because the copper grid, covered by a thick layer of Formvar/carbon layer and sealed in the nafion network, is not directly accessible to the solution, which largely slows down or even prevents it from oxidation. Nevertheless, interestingly, the FCCG-GCE demonstrated some catalytic effect toward reduction of H_2O_2 because the reduction current *I* is evidently enhanced in the presence of 2.45 mM H_2O_2 (curve 2, Figure 9c) compared with those in the absence of H_2O_2 (curve 1, Figure 9c).

The CVs of the Au-FCCG-GCE (curves 3 and 4, Figure 9c) are clearly differentiated from those of the FCCG-GCE. A cathodic peak centered at −0.165 was observed in the CV without addition of H_2O_2 in the PBS (curve 3, Figure 9c), which should be assigned to the reduction of Cu_2O/CuO.[35,36] In the presence of 2.45 mM H_2O_2, the CV pattern (curve 4, Figure 9c) changes significantly so that the reduction current is greatly enhanced compared with the case without H_2O_2 and no defined cathodic or anodic peaks are observed. This is similar to those given by Au-based H_2O_2 sensors[37] but different from those from the Cu_2O/CuO-based ones.[36,38] We attribute the significantly enhanced electrocatalytic activity of Au-FCCG-GCE mainly to the presence of the surface Au nanofractals, considering that the Cu_2O/CuO aggregates formed during the preparation of Au-FCCG mainly locate on the copper-grid side which as discussed previously cannot be accessed directly by the reactant solute. Notably, the intensity of the reduction current obtained by the Au-FCCG-GCE is much higher than that of the FCCG-GCE under the same operating conditions (i.e., at the same voltage and the same H_2O_2 concentration). For instance, at −0.2 V, the reduction current in the forward scan for the Au-FCCG-GCE is 9.2 times that of the FCCG-

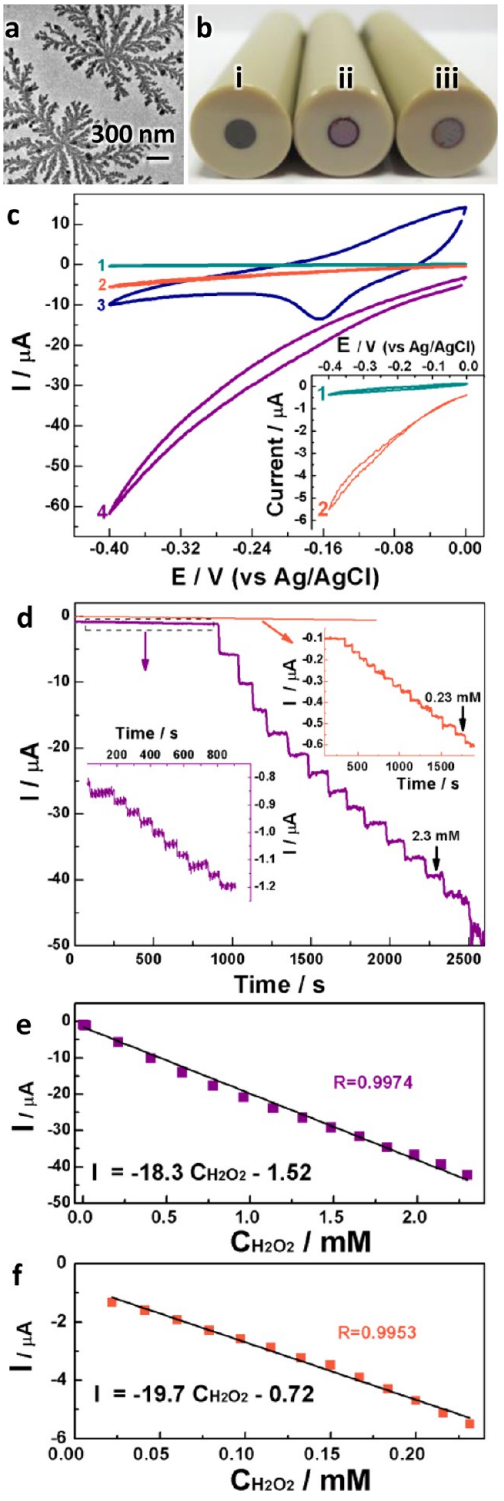

Figure 9. (a) Au nanofractals for H_2O_2 sensing. (b) Photographs of (i) a bare GCE, (ii) a FCCG-GCE, and (iii) a Au-FCCG-GCE. (c) CVs of FCCG-GCE (curves 1 and 2 and the inset) and the Au-FCCG-GCE (curves 3 and 4), where curves 1 and 3 were measured in absence of H_2O_2 and curves 2 and 4 were measured in the presence of H_2O_2. (d) Chronoamperometric responses of Au-FCCG-GCE (purple curves) and FCCG-GCE (orange curves) to successive additions of H_2O_2. The purple inset details the segment of the curve framed with a rectangle. (e and f) Plots of electrocatalytic current (*I*) vs H_2O_2 concentration ($C_{H_2O_2}$) for (e) Au-FCCG-GCE and (f) FCCG-GCE.

DOI: 10.1021/acsami.5b06818
ACS Appl. Mater. Interfaces 2015, 7, 21552−21561

GCE. Such results clearly verified the important role of the presence of the Au nanofractals in the Au-FCCG-GCE.

The chronoamperometric responses of the two above electrodes to successive additions of H_2O_2 are shown in Figure 9d. The FCCG-GCE responds rapidly to the addition of H_2O_2 up to a concentration of 0.23 mM. The linear range of FCCG-GCE ranges from 21.7 μM to 0.23 mM (Figure 9f) with a correlation coefficient of 0.9953 (n = 13), and the sensitivity of the FCCG-GCE is 278.8 μA mM^{-1} cm^{-2}. In general, the Au-FCCG-GCE behaves quite differently from the FCCG-GCE. It responds rapidly and achieves steady-state current in less than 8 s to successive additions of H_2O_2 up to a concentration of 2.3 mM H_2O_2 (purple curve, Figure 9d). As shown in Figure 9e, a wide linear range was obtained ranging from 2.0 μM to 2.3 mM with a correlation coefficient of 0.9974 (n = 22). The sensitivity is 259 $\mu A m M^{-1} cm^{-2}$, and the detection limit is 0.156 μM at the signal-to-noise of 3. Such an overall performance is comparable to or even outperforms many Au- and/or Cu-based composite electrochemical sensors reported in the literature.[35,37,39,40] As an "inert" noble metal, the catalytic activity of Au-based nanocatalysts closely relates with their sizes. First, the high electrocatalytic activity of our Au-FCCG-GCE toward the reduction of H_2O_2 associates with the ultrasmall diameter and polycrystalline nature of the Au nanobranches within the nanofractals. Second, one can expect that numerous tiny integrated wires in the in situ formed Au nanofractals must have a higher electrical conductivity compared with those of less-connected Au nanoparticles. Third, because there is no overlap among the Au nanofractals compared with paste-based sensing electrodes, the thoroughly exposed surfaces of Au nanofractals can be accessed easily with a low diffusion barrier by the analyte molecules.

4. CONCLUSIONS

2D Au nanofractals with branches as fine as 4.0 nm in diameter and lengths up to micrometers have been successfully realized via an IGR strategy in which the cathodic and anodic reactions are separated in space by a conducting film. The successful formation of such fine Au nanofractals relies on usage of an IGR setting with inherent electrical resistance in the conducting film and Au(I) species with a relatively low standard oxidation potential, which enables the realization of slow reduction kinetics. With this approach, the growth density, the deposition location, and local features of the as-formed gold nanofractals can also be modulated, further illustrating good control over the reduction kinetics and thus the morphology of product. This work contributes to both fabrication of fine metal fractal structures and mechanistic investigations of interfacial galvanic replacement reactions. Au nanofractals grown on FCCG have also been employed for fabrication of electrochemical sensors that demonstrate excellent performance in sensing H_2O_2 with a relatively wide linear range, high sensitivity, and low detection limit.

■ ASSOCIATED CONTENT

Supporting Information

The Supporting Information is available free of charge on the ACS Publications website at DOI: 10.1021/acsami.5b06818.

UV−vis spectra, XPS spectra, FESEM images, and TEM images of studied samples, and photographs of FCCG-GCE electrodes. (PDF)

■ AUTHOR INFORMATION

Corresponding Author

*E-mail: chezhc@nus.edu.sg.

Notes

The authors declare no competing financial interest.

■ ACKNOWLEDGMENTS

Y.Z. thanks NUS Graduate School for Integrative Sciences and Engineering for providing her postgraduate scholarship. We thanks Dr. Chun Xian Guo for his helpful discussion on sensing measurements. We also gratefully acknowledge NUS and GSK Singapore for financial support. This project is also partially funded by the National Research Foundation (NRF), Prime Minister's Office, Singapore under its Campus for Research Excellence and Technological Enterprise (CREATE) program.

■ REFERENCES

(1) Tokuyama, M.; Kawasaki, K. *Phys. Lett. A* **1984**, *100*, 337.
(2) Nittmann, J.; Daccord, G.; Stanley, M. *Nature* **1985**, *314*, 141.
(3) Witten, T., Jr; Sander, L. M. *Phys. Rev. Lett.* **1981**, *47*, 1400.
(4) Bai, X.; Zheng, L. *Cryst. Growth Des.* **2010**, *10*, 4701.
(5) Pan, M.; Sun, H.; Lim, J. W.; Bakaul, S. R.; Zeng, Y.; Xing, S.; Wu, T.; Yan, Q.; Chen, H. *Chem. Commun.* **2012**, *48*, 1440.
(6) Qin, Y.; Song, Y.; Sun, N.; Zhao, N.; Li, M.; Qi, L. *Chem. Mater.* **2008**, *20*, 3965.
(7) Han, X.; Wang, D.; Huang, J.; Liu, D.; You, T. *J. Colloid Interface Sci.* **2011**, *354*, 577.
(8) Meyre, M.-E.; Lambert, O.; Faure, C. *J. Mater. Chem.* **2006**, *16*, 3552.
(9) Zhou, Y.; Wang, H.; Lin, W.; Lin, L.; Gao, Y.; Yang, F.; Du, M.; Fang, W.; Huang, J.; Sun, D.; et al. *J. Colloid Interface Sci.* **2013**, *407*, 8.
(10) Lu, X.; Yavuz, M. S.; Tuan, H.-Y.; Korgel, B. A.; Xia, Y. *J. Am. Chem. Soc.* **2008**, *130*, 8900.
(11) Liu, X.; Wu, N.; Wunsch, B. H.; Barsotti, R. J.; Stellacci, F. *Small* **2006**, *2*, 1046.
(12) Huang, T.; Meng, F.; Qi, L. *Langmuir* **2010**, *26*, 7582.
(13) Liu, J.; Fu, Y.; Guo, A.; Wang, C.; Huang, R.; Zhang, X. *J. Phys. Chem. C* **2008**, *112*, 4242.
(14) Feng, J.-J.; Li, A.-Q.; Lei, Z.; Wang, A.-J. *ACS Appl. Mater. Interfaces* **2012**, *4*, 2570.
(15) Huang, J.; Han, X.; Wang, D.; Liu, D.; You, T. *ACS Appl. Mater. Interfaces* **2013**, *5*, 9148.
(16) Fang, J.; Ma, X.; Cai, H.; Song, X.; Ding, B. *Nanotechnology* **2006**, *17*, 5841.
(17) Vazquez, L.; Salvarezza, R.; Ocón, P.; Herrasti, P.; Vara, J.; Arvia, A. *Phys. Rev. E: Stat. Phys., Plasmas, Fluids, Relat. Interdiscip. Top.* **1994**, *49*, 1507.
(18) Zhang, H.; Jin, M.; Wang, J.; Li, W.; Camargo, P. H.; Kim, M. J.; Yang, D.; Xie, Z.; Xia, Y. *J. Am. Chem. Soc.* **2011**, *133*, 6078.
(19) Kim, K. W.; Kim, S. M.; Choi, S.; Kim, J.; Lee, I. S. *ACS Nano* **2012**, *6*, 5122.
(20) Sun, Y.; Xia, Y. *J. Am. Chem. Soc.* **2004**, *126*, 3892.
(21) Oh, M. H.; Yu, T.; Yu, S.-H.; Lim, B.; Ko, K.-T.; Willinger, M.-G.; Seo, D.-H.; Kim, B. H.; Cho, M. G.; Park, J.-H.; et al. *Science* **2013**, *340*, 964.
(22) Chen, X.; Cui, C. H.; Guo, Z.; Liu, J. H.; Huang, X. J.; Yu, S. H. *Small* **2011**, *7*, 858.
(23) Gutés, A.; Carraro, C.; Maboudian, R. *J. Am. Chem. Soc.* **2010**, *132*, 1476.
(24) Liu, R.; Sen, A. *Chem. Mater.* **2012**, *24*, 48.
(25) Mikhlin, Y.; Likhatski, M.; Karacharov, A.; Zaikovski, V.; Krylov, A. *Phys. Chem. Chem. Phys.* **2009**, *11*, 5445.
(26) Kuo, C. L.; Huang, M. H. *J. Phys. Chem. C* **2008**, *112*, 11661.
(27) Schwartzberg, A.; Grant, C.; Van Buuren, T.; Zhang, J. *J. Phys. Chem. C* **2007**, *111*, 8892.
(28) Yao, K. X.; Yin, X. M.; Wang, T. H.; Zeng, H. C. *J. Am. Chem. Soc.* **2010**, *132*, 6131.

DOI: 10.1021/acsami.5b06818
ACS Appl. Mater. Interfaces 2015, 7, 21552−21561

(29) Khattak, G.; Mekki, A.; Wenger, L. *J. Non-Cryst. Solids* **2004**, *337*, 174.
(30) Yao, K. X.; Liu, X.; Zhao, L.; Zeng, H. C.; Han, Y. *Nanoscale* **2011**, *3*, 4195.
(31) Pang, M.; Hu, J.; Zeng, H. C. *J. Am. Chem. Soc.* **2010**, *132*, 10771.
(32) Bocharov, G. S.; Eletskii, A. V. *Nanomaterials* **2013**, *3*, 393.
(33) Pérez-Juste, J.; Liz-Marzan, L.; Carnie, S.; Chan, D. Y.; Mulvaney, P. *Adv. Funct. Mater.* **2004**, *14*, 571.
(34) Liu, M.; Guyot-Sionnest, P. *J. Phys. Chem. B* **2005**, *109*, 22192.
(35) Ashok Kumar, S.; Lo, P.-H.; Chen, S.-M. *J. Electrochem. Soc.* **2009**, *156*, E118.
(36) Zhang, L.; Li, H.; Ni, Y.; Li, J.; Liao, K.; Zhao, G. *Electrochem. Commun.* **2009**, *11*, 812.
(37) Jia, J.; Wang, B.; Wu, A.; Cheng, G.; Li, Z.; Dong, S. *Anal. Chem.* **2002**, *74*, 2217.
(38) Li, S.; Zheng, Y.; Qin, G. W.; Ren, Y.; Pei, W.; Zuo, L. *Talanta* **2011**, *85*, 1260.
(39) Zhang, J.; Oyama, M. *Electrochim. Acta* **2004**, *50*, 85.
(40) Fang, Y.; Guo, S.; Zhu, C.; Zhai, Y.; Wang, E. *Langmuir* **2010**, *26*, 11277.

DOI: 10.1021/acsami.5b06818
ACS Appl. Mater. Interfaces 2015, 7, 21552−21561